Ultrasonics Sonochemistry 101 (2023) 106717

Contents lists available at ScienceDirect

Ultrasonics Sonochemistry

journal homepage: www.elsevier.com/locate/ultson

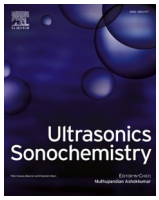

Joint effects of gas bubbles and solid particles on sonochemical inhibition in sonicated aqueous solutions

Kunpeng Su [a,b], Binghui Li [a], Jianhua Wu [a,*], Pei Xin [b,c], Shangtuo Qian [d]

[a] College of Water Conservancy and Hydropower Engineering, Hohai University, Nanjing 210098, China
[b] State Key Laboratory of Hydrology–Water Resources and Hydraulic Engineering, Hohai University, Nanjing 210098, China
[c] Yangtze Institute for Conservation and Development, Hohai University, Nanjing 210098, China
[d] College of Agricultural Science and Engineering, Hohai University, Nanjing 210098, China

ARTICLE INFO

Keywords:
Sonochemical effect
Solid particles
Gas bubbles
Ultrasound attenuation

ABSTRACT

Wastewater is a multicomponent and multiphase mixture. Gas bubbles and solid particles in the dispersed phase influence sonochemical efficiency during ultrasonic treatment of wastewater, sometimes unfavorably; however, the influencing factors and mechanisms remain unclear. In this paper, the influence of argon gas bubbles (1.2 mm) and monodisperse silica particles (0.1 mm) on sonochemical effects in an aqueous system using a horn-type reactor (20 kHz) is reported. Triiodide formation decreased with an increase in the volume fraction of either or both phases. The two phases started inhibiting sonoreactions as the total volume fraction approached 3.0–4.0 vol % compared to pure water. The effect of the gas-to-solid ratio is also considered. We propose an acoustic attenuation model, which incorporates the scattering effect of solid particles and the thermal effect of gas bubbles. The agreement between the modeling and experimental results demonstrates that the two phases are jointly responsible for sonochemical inhibition by increasing ultrasound attenuation. This enhances the understanding of sonochemistry in gas–solid–liquid systems and helps regulate gases and solids in sonochemical reactors.

1. Introduction

Since early research in sonochemistry, power ultrasound application has been a subject of growing interest in wastewater treatment and environmental remediation areas [1–3]. When cavitation bubbles generated by ultrasound oscillate and collapse, hydroxyl radicals (·OH) are produced owing to the ultrahigh temperature and pressure inside the bubbles [4]. These highly reactive species are crucial in the oxidative destruction of non-biodegradable organic pollutants in the aqueous phase. Ultrasound treatment is a simple technique, requiring only electrical energy; however, scaling up requires the knowledge of all possible factors that influence sonoreactions [5–7]. For example, besides organic compounds, wastewater also contains inorganic contaminants such as sediment and microplastics [8], as well as undissolved gas bubbles [9]. These rigid particles and deformable bubbles may influence the efficiency of the sonochemical reactors that operate prior to biological (secondary) treatment [10,11], as primary treatment removes only ~60% of suspended solids [12] and biological treatment requires aeration processes [13]. Therefore, particular attention must be given to the sonochemical effects in gas–solid–liquid mixtures.

Several studies have investigated sonochemical activity in solid particle suspensions [14–22] and in bubbly liquids [23–26] and are mostly concerned with how the quality and quantity of these solid/gas phases influence bubble characteristics and sonoreactions. Surface roughness, size, and shape are the most-studied indicators of particle quality. Irregularly shaped particles with rough surfaces may improve ·OH yields [27], according to the crevice model [28]. Large particles can induce asymmetric bubble collapse and form high-speed micro-jets that impact the surface, whereas small ones may be propelled by the shock waves from bubble collapse and collide with one another [29–32]. In both cases, defects form on the surface and may act as nucleation sites. In the presence of the gaseous phase, the intrinsic nature of gases (e.g., polytropic index, solubility, and chemical reactivity) has been recognized as a major factor influencing sonochemistry. Monatomic gases can raise the temperature within the collapsing bubbles owing to high polytropic index [33], whereas diatomic gases such as oxygen and nitrogen can directly participate in reactions that promote or prevent radical production [34]. By cushioning bubble collapse with enhanced gas

* Corresponding author.
E-mail address: jhwu@hhu.edu.cn (J. Wu).

https://doi.org/10.1016/j.ultsonch.2023.106717
Received 13 October 2023; Received in revised form 2 December 2023; Accepted 5 December 2023
Available online 10 December 2023

diffusion [35] and preventing bubble coalescence with decreased pH values [36], carbon dioxide inhibits radical production. Previous research has also demonstrated the sequence of radical production among different gases [37,38] or gas mixtures [39,40].

The quantity of the solid/gas phases exerts a decisive influence besides the physical and chemical qualities. Katekhaye and Gogate [41] studied the sonochemical activity in 0.2–0.6-vol% suspensions of titania powder and reported higher ·OH yields than in water; the yields increased with solids fraction. They ascribed this to additional nucleation sites, as well as titania's catalytic activity [42]. Her et al. [43] found that ·OH yields in 3–12-vol% glass bead suspensions were lower than those in water, and decreased with increasing solids fraction, which tallied with the results of other studies [44,45]. In more concentrated suspensions, gas/vapor diffusing through the bubble wall would be harder, which would in turn make it harder for bubbles to oscillate or collapse [46]. Tuziuti et al. [47] reported an improved sono-oxidation rate in the presence of micron-sized air bubbles. They suggested that further dissolved air was the probable cause, which led to additional cavitation bubbles [48]. Choi et al. [49] investigated the influence of the air bubbling rate on sonodegradation and discovered that ·OH yields first increased and subsequently decreased with increasing air bubbling rates (0–16 $L{\cdot}min^{-1}$). Gogate et al. [50,51] and Xia et al. [52] also observed similar trends. Cushioned bubble collapse and increased compressibility were deemed responsible for reduced cavitation intensity with higher air concentrations [53,54]. Although examining how the quantities of the solid and gas phases affect sonoreactions in gas–solid–liquid mixtures is important, the combined effects have rarely been studied.

The consensus regarding the mechanism is that gas bubbles and solid particles can bring about points of weakness in the liquid continuum, lowering the cavitation threshold and leading to additional radical production. The only difference is that the cavitation nuclei in bubbly liquids are directly the free tiny bubbles [52], whereas the ones that solid particles cause are the undissolved gas adhering to the particle surface, e.g., in a cleft or crevice [28]. However, consensus regarding why the gas and solid phases inhibit sonoreactions in certain circumstances is lacking. Extensive evidence has demonstrated the attenuation of acoustic waves that propagate through solids suspensions [55–57] or bubbly liquids [58–60]. This could be a rational explanation since reduced ultrasound intensity makes it harder for cavitation inception to occur and bubbles to form. Although various attenuation regimes in the presence of gas or solid phases have been identified, limited studies touch upon the relation between sonochemical inhibition and ultrasound attenuation in gas–solid–liquid mixtures.

This study aimed to examine the sonochemically inhibiting effects of the gas and solid phases and clarify the underlying mechanisms. Sonochemical experiments were performed in aqueous solutions containing argon gas bubbles and silica particles and the experimental results were analyzed using an integrated ultrasound attenuation model.

2. Materials and methods

2.1. Materials

Analytical grade potassium iodide (KI), luminol ($C_8H_7N_3O_2$), and potassium hydroxide (KOH) were acquired from Beilian Fine Chemical Development Co., Ltd. (Tianjin, China), Haohong Biomedical Technology Co., Ltd. (Shanghai, China), and Jinshan Chemical Reagent Co., Ltd. (Chengdu, China), respectively. All chemicals were used as received.

Argon, the cheapest noble gas, was selected as the gas phase owing to its ability to produce higher sonochemical activity than polyatomic gases [5]. Cylinders storing high-purity grade argon were supplied by Qiaopai Technology Development Co., Ltd. (Nanjing, China). Silica particles with a uniform diameter of 0.1 mm (density: 2.4×10^3 $kg{\cdot}m^{-3}$) were used as the solid phase, provided by Tokyo Chemical Industry Co., Ltd. (Tokyo, Japan). The monodispersity in silica particle size was confirmed using a scanning electron microscope (Regulus 8100, Hitachi High-Tech Corp., Japan), as shown in Fig. 1.

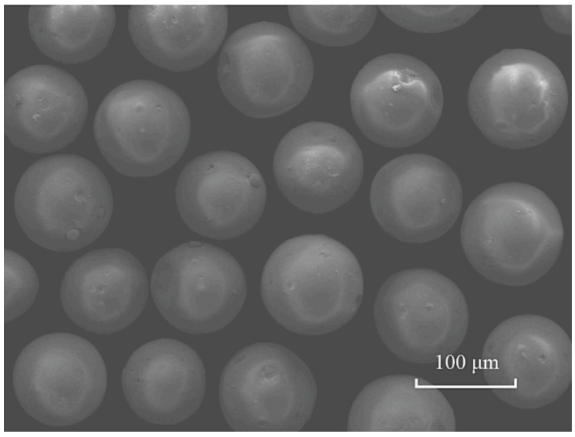

Fig. 1. Image of monodisperse silica particles captured using a scanning electron microscope.

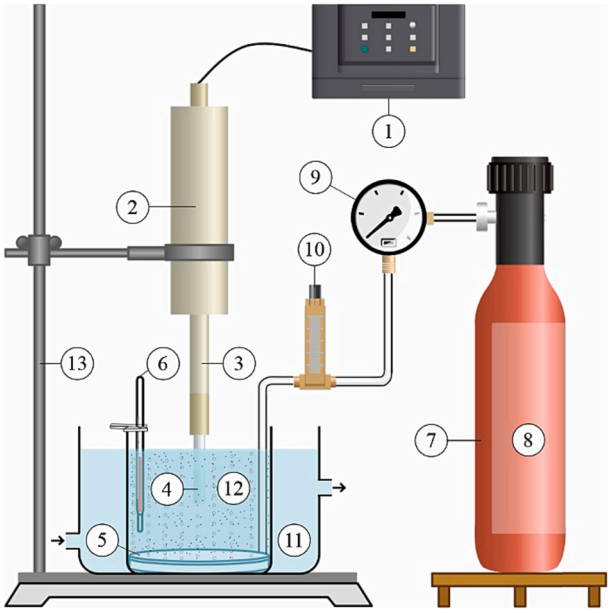

Fig. 2. Schematic of the experimental setup. Key: 1: ultrasonic generator, 2: piezoelectric transducer, 3: ultrasonic horn, 4: output tip, 5: fine bubble diffuser, 6: thermometer, 7: gas cylinder, 8: argon (inside), 9: pressure-reducing regulator, 10: rotameter, 11: cooling bath, 12: test solution containing argon gas bubbles and/or silica particles, and 13: supporting rod.

2.2. Experimental setup

A 20-kHz horn-type reactor equipped with a piezoelectric transducer (VCY−1500, Shanghai Y&Y Sonic) was employed (Fig. 2). Ultrasound was generated with an applied electric power of 250 W, and the absorbed acoustic power was approximately 135 W (measured using the thermal probe method [61]). The ultrasonic horn, made of Ti-6Al-4V titanium alloy, was placed erect at the center of a cylindrical PET vessel (inner radius: 6.0 cm). The horn tip surface was submerged 5.0 cm beneath the free surface of the test solution, transferring the acoustic energy from the transducer into the solution. The solution temperature was monitored using an alcohol thermometer and maintained at 25 ± 1 °C by positioning the vessel in a circulating water bath as horn heating was inevitable.

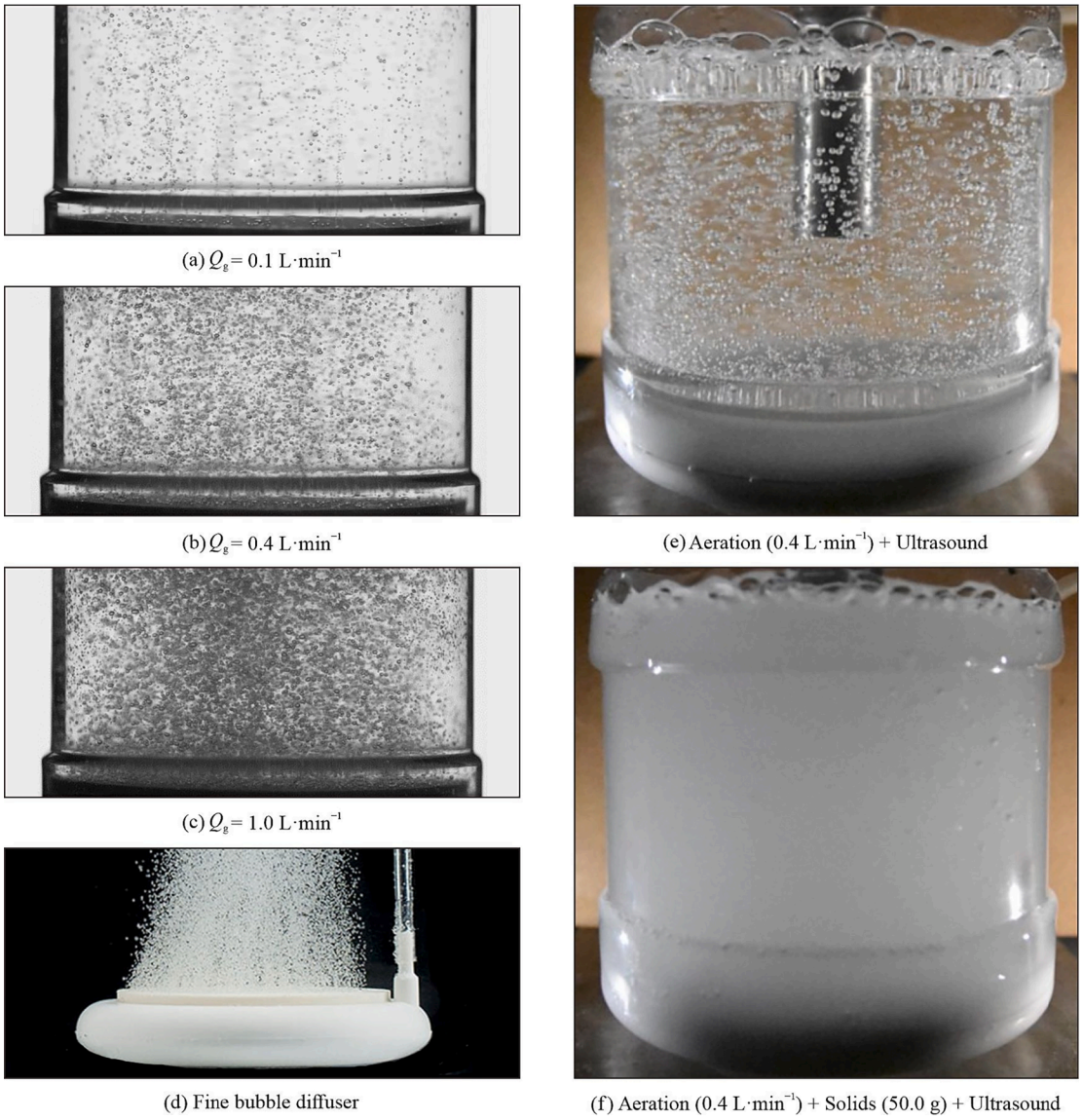

Fig. 3. Images showing the rise of gas bubbles at different gas flow rates with no solids or ultrasound: (a) $Q_g = 0.1$ L·min^{-1}, (b) $Q_g = 0.4$ L·min^{-1}, and (c) $Q_g = 1.0$ L·min^{-1} after being released from (d) a ceramic media diffuser (effective aeration diameter: 10.0 cm); and gas bubbling at $Q_g = 0.4$ L·min^{-1} under sonication (e) without solids and (f) with 50.0-g suspended silica particles.

A disc-shaped fine-pore ceramic diffuser was installed at the bottom of the vessel to continuously supply argon to the test solution, producing a plethora of rising gas bubbles (Fig. 3a–d). The volume of gas bubbles in the solution (V_g) at a specific point in time could be calculated based on the rise of the liquid surface caused by aeration (Δh), i.e., $V_g = S\Delta h$, where S is the vessel's cross-sectional area. For example, $V_g \approx 11.3$, 22.6, 33.9, 45.2, and 56.5 mL when $\Delta h = 0.1$, 0.2, 0.3, 0.4, and 0.5 cm, respectively. Volumetric gas flow rates (Q_g) were regulated using a pressure-reducing valve (F60–0085, Foshan Feibao Tools) and measured using a rotameter (LZB–3WB, Hangzhou Darhor Tech.). V_g could be controlled during the tests by altering Q_g owing to the linear correlation between V_g and Q_g (Fig. 4). The average diameter of the gas bubbles was approximately 1.2 mm under typical operating conditions, determined from the images recorded by a high-speed camera (Phantom VEO 1010, Vision Research) at 10,000 fps. Owing to ultrasonic agitation, the gas bubbles were more evenly distributed in the sonicated solution (Fig. 3e) than in the solution without sonication (Fig. 3b).

To avoid floc clogging of the gas-release orifices in the porous ceramics, routine removal of fouling materials was required, and the operation of the aeration system should be started before adding silica. The silica particles were observed to remain in suspension in sonicated aerated solutions (Fig. 3f) thanks to the downward forces caused by ultrasonic agitation and upward forces due to diffused aeration. The suspended particles moved vigorously in a random manner owing to the intense mixing. Thus, it seems reasonable to assume that the silica particles were well distributed throughout the vessel. The interaction between bubbles and particles, as well as their mutual influence in terms of size distribution and movement, was neglected, since the gas bubbles were supplied continuously and much larger in size. The volume of silica particles in the solution (V_s) was calculated as $V_s = m_s/\rho_s$, in which m_s and ρ_s are the mass and density of silica particles, respectively. An electronic balance was used to weigh the particles. All particles were unrecycled after every test completion, due to the inevitable reduction in the particle size that sonication might induce [32].

2.3. Measuring sonochemical yield

The KI dosimetry method was used to quantify the amount of ·OH generated by acoustic cavitation. In this method, ·OH oxidized a fraction of iodide ions (I^-) to generate molecular iodine (I_2), and the remaining

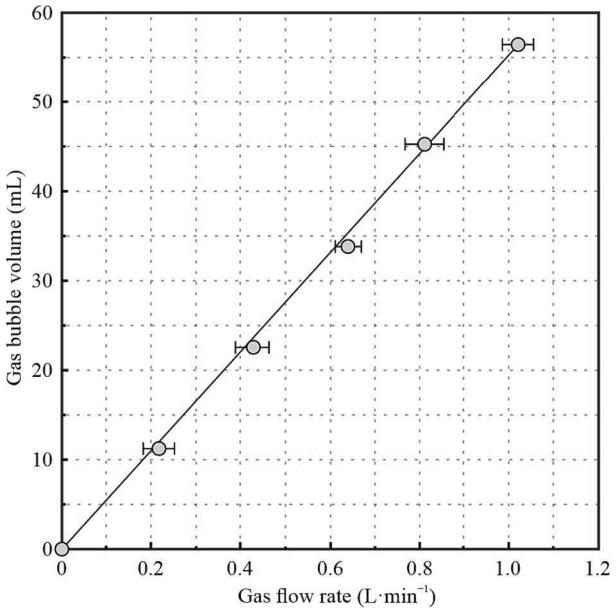

Fig. 4. Variation of gas bubble volume with the gas flow rate. The error bars represent one standard deviation.

I^- reacted with I_2 to form the triiodide ion (I_3^-). The maximum absorption of I_3^- was at a wavelength of 355 nm [62], and the adsorption of I_3^- on the surfaces of the vessel, diffuser, and silica particles was neglected. Just before each test, aqueous KI solutions (0.1 mol·L^{-1}) were freshly prepared using distilled water (air-saturated), with the basicity adjusted to a pH of 8 using KOH. Despite the initial presence of dissolved air in the solution, the effect of dissolved oxygen concentration on I_3^- production was neglected because of the continuous argon gas bubbling and the degassing effect induced by ultrasonic irradiation [63].

The duration of each test was 25 min. An aliquot of solution (6–7 mL) containing minimal bubbles and particles was sampled at regular intervals to establish ·OH yield versus time curves. It was centrifuged at 2500 rpm for 2 min and left undisturbed for 5 min. The supernatant was subsequently transferred into quartz cuvettes for spectrophotometric analysis, using an ultraviolet–visible spectrophotometer (UV754N, Shanghai Aucy Scientific Instrument). The I_3^- concentration generated, $c(I_3^-)$, was determined according to the Beer–Lambert law: $c(I_3^-) = A/(\varepsilon w)$, where A is the measured absorbance, ε is the molar attenuation coefficient (ε = 23200 L•mol^{-1}•cm^{-1}), and w is the width of each cuvette (w = 1.0 cm). The procedure was repeated throughout the test at 5 min increments. Each test was repeated three times, and the mean values were used in the subsequent analyses.

To visualize the sonochemically active zone under the argon gas bubbling conditions, the sonochemiluminescence (SCL) method was also utilized. SCL images were obtained using an aqueous solution of luminol (1 mmol·L^{-1}) and KOH (0.1 mol·L^{-1}), captured with a digital camera (D3400, Nikon) in total darkness. The shutter speed was fixed at 30 s (exposure time).

2.4. Experimental cases

For three-phase gas–solid–liquid mixtures, the gas volume fraction, φ_g, and the solids fraction, φ_s, are defined as follows:

$$\varphi_g = \frac{V_g}{V_g + V_s + V_l} \quad (1)$$

$$\varphi_s = \frac{V_s}{V_g + V_s + V_l} \quad (2)$$

where V_g, V_s, and V_l are the respective volumes of the gas, solid, and liquid phases, respectively. In this study, V_l was unchanging (V_l = 1.1 L) as the distance from the initial surface of the additive-free solution to the ceramic diffuser was always set to 9.6 cm. The fraction of the total volume that is made up of gas bubbles and solid particles, φ_{total}, and the gas-to-solid ratio, λ_φ, i.e., the ratio of φ_g to φ_s, are the other two parameters of interest. Volume fraction of the liquid phase is denoted by $\varphi_l = 1 - \varphi_{total}$.

Table 1
Experimental cases (gas–solid–liquid mixtures).

Case No.	φ_g[a] (vol %)	φ_s[b] (vol %)	φ_{total}[c] (vol%)	λ_φ[d]	V_g[e] (mL)	Q_g[f] (L·min^{-1})	V_s[g] (mL)	m_s[h] (g)
1	1.0	1.0	2.0	1:1	11.1	0.212	11.1	26.6
2	1.5	1.5	3.0	1:1	16.8	0.315	16.8	40.3
3	2.0	2.0	4.0	1:1	22.6	0.419	22.6	54.3
4	3.0	3.0	6.0	1:1	34.7	0.636	34.7	83.2
5	1.0	2.0	3.0	1:2	11.2	0.214	22.4	53.7
6	2.0	1.0	3.0	2:1	22.4	0.415	11.2	26.9
7	1.0	3.0	4.0	1:3	11.3	0.216	33.9	81.4
8	3.0	1.0	4.0	3:1	33.9	0.623	11.3	27.1
9	1.0	5.0	6.0	1:5	11.6	0.220	57.8	138.6
10	5.0	1.0	6.0	5:1	57.8	1.051	11.6	27.7

[a] φ_g—volume fraction of the argon gas bubbles.
[b] φ_s—volume fraction of the silica particles.
[c] φ_{total}—total volume fraction of the argon gas bubbles and silica particles (sum of φ_g and φ_s).
[d] λ_φ—gas-to-solid ratio (ratio of φ_g to φ_s).
[e] V_g—volume of the argon gas bubbles.
[f] Q_g—volumetric gas flow rate.
[g] V_s—volume of the silica particles.
[h] m_s—mass of the silica particles.

Twenty-three experimental cases were performed, including ten three-phase cases in which gas bubbles and solid particles coexisted (Table 1), twelve two-phase cases with only gas bubbles (φ_g = 0.5, 1.0, 1.5, 2.0, 3.0, or 5.0 vol%) or only solid particles (φ_s = 0.5, 1.0, 1.5, 2.0, 3.0, or 5.0 vol%), and a single-phase case (pure water) for reference. Through the three-phase cases, we investigated the effects of the total volume fraction (Cases 1–4: φ_{total} = 2.0–6.0 vol%, λ_φ = 1:1) and the gas-to-solid ratio (Cases 2, 5, and 6: φ_{total} = 3.0 vol%, λ_φ = 1:2 to 2:1; Cases 3, 7, and 8: φ_{total} = 4.0 vol%, λ_φ = 1:3 to 3:1; and Cases 4, 9, and 10: φ_{total} = 6.0 vol%, λ_φ = 1:5 to 5:1). The Q_g values for all the cases listed in Table 1 were determined by interpolation based on known data points in Fig. 4, owing to the strong positive correlation between V_g and Q_g.

3. Results

I_3^- production linearly increased with ultrasonic irradiation time in the test solution containing either silica particles or argon gas bubbles, as well as in the single-phase case (Fig. 5), which is well aligned with the results of past studies [45,52]. This indicates that the formation rate of I_3^-, $r_f(I_3^-)$, defined as the increase in I_3^- concentration per unit time, was independent of the irradiation time (≤25 min). In both kinds of two-phase mixtures, the sonochemical yields after ultrasonic irradiation for 25 min attained the smallest value at the highest φ_s or φ_g (5.0 vol%) and the largest value at the lowest φ_s or φ_g (0.5 vol%), where more I_3^- was detected at every time point compared with the pure water scenario. A one-quarter reduction in I_3^- production was observed at 25 min with the solid or gas phase being added from 0.5 vol% to 5.0 vol%, reflecting the sonochemically inhibiting effects of these additives.

Despite the similarity in reaction inhibition at high φ_s or φ_g, considerable differences existed between the silica particles and argon gas bubbles in influencing sonochemistry. Adding argon gas bubbles at φ_g = 0.5 vol% generated 17% more I_3^- than that in the pure water case (Fig. 5b) and 8% more than that in the 0.5-vol% suspensions of the silica particles (Fig. 5a). This implies that the 1.2-mm gas bubbles had stronger enhancing capability than the 0.1-mm solid particles when φ_s

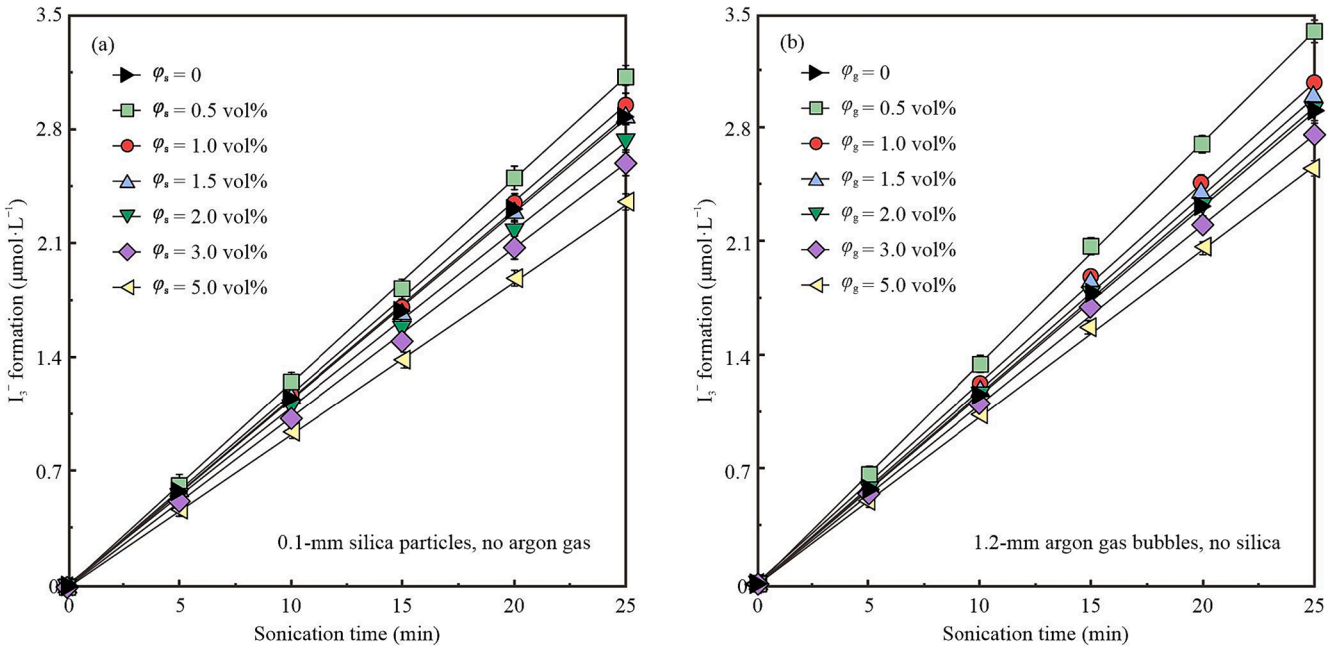

Fig. 5. I_3^- concentration plotted against sonication time for two-phase mixtures containing (a) 0.1-mm silica particles (volume fraction φ_s = 0.5–5.0 vol%), and (b) 1.2-mm argon gas bubbles (volume fraction φ_g = 0.5–5.0 vol%), as well as for the aqueous solution. Error bars are shown when they are larger than the data point markers.

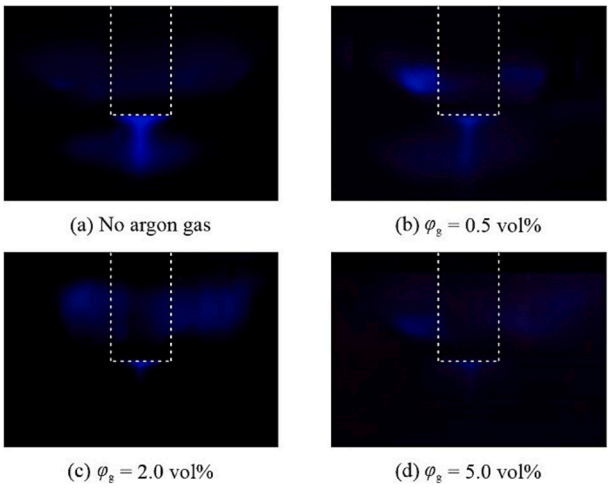

Fig. 6. Sonochemiluminescence images showing sonochemically active zones (a) without aeration, and at different gas volume fractions: (b) φ_g = 0.5 vol%, (c) φ_g = 2.0 vol%, and (d) φ_g = 5.0 vol%. The dashed line represents the location of the vibrating horn.

= φ_g, even though the number of particles was considerably greater than that of the gas bubbles. The main reason may be the different nuclei-introducing abilities of the two phases. Additionally, silica particle introduction at φ_s = 1.5 vol% started to inhibit I_3^- formation, which was slightly less than that in the pure water case (Fig. 5a). Contrastingly, the argon gas bubbles had an overall enhancing effect on I_3^- formation when φ_g = 1.5 vol% (Fig. 5b). The inhibitory effect of the gas bubbles began to be dominant merely when φ_g was doubled to 3.0 vol%, demonstrating the strong capability of the gas bubbles in nucleus introduction and sonochemical enhancement. Although the sonochemically enhancing mechanisms of the gas bubbles and solid particles differ, their inhibitory effects at high volume fractions exhibited some similarities, implying similar mechanisms in reducing sonochemical yields.

The inhibitory effect of gas bubbles was also visualized using the luminol method (Fig. 6). The SCL image under the non-aeration condition (Fig. 6a) was similar to the findings reported by Son et al. [64]. High-intensity SCL light was detected beneath the horn tip, with lower-intensity light shining above the vessel bottom and around the immersed horn. Interestingly, compared with the non-aeration condition, the region under the horn got darker when φ_g = 0.5 vol% (Fig. 6b). This may be because the large gas bubbles rising from the bottom induced mixing and modified the local sound energy field [25], inhibiting ultrasound transmission and resulting in limited active zones. The higher SCL intensity in the circular zone around the horn (Fig. 6b), however, might result from the introduction of additional nuclei. Although I_3^- production at φ_g = 0.5 vol% was higher than that in the pure water scenario (Fig. 5b), no significant increase in the total SCL intensity was observed, possibly due to the disturbance the rising gas bubbles caused to the capturing of emitted light [49]. As φ_g further increased, a decrease in the intensity of SCL light was noticed in the active zones (Fig. 6c and d), demonstrating the sonochemically inhibiting effect of the gas bubbles.

We can first adopt an effective-medium approach to analyze the sonochemical effects in gas–solid–liquid mixtures. This implies assuming the solid–liquid mixture as a continuous medium, where gas bubbles are additives, or considering the gas bubbles and the liquid as a whole with solid particles as additives. In Fig. 7(a) and (b), the bubbly solution with φ_g = 1.0 vol% and the 1.0-vol% solid particle suspension were treated as effective media, respectively. Data in both figures follow the same "first increasing then decreasing" pattern of $r_f(I_3^-)$ against the volume fraction of the additives. This result is extremely similar to the results of the two-phase cases (Fig. 5), and the only difference is that the gas/solid phase in the effective medium altered the nucleation characteristics of the medium. For instance, adding argon gas bubbles with φ_g from 1.0 to 5.0 vol% into the silica suspension (φ_s = 1.0 vol%) caused a less sharp decrease in $r_f(I_3^-)$ compared to when silica particles were added into the bubbly solution (φ_g = 1.0 vol%) with φ_s from 1.0 to 5.0 vol%. This indicates that the gas phase in the effective medium performed better in introducing nuclei, enhancing sonochemical activity, and offsetting the inhibitory effect of the additives.

Fig. 7(c)–(f) shows the experimental data for the three-phase cases in terms of different φ_{total} or λ_φ. Of all the three-phase cases in Table 1, the highest and lowest I_3^- formation rates occurred in Cases 1 and 4,

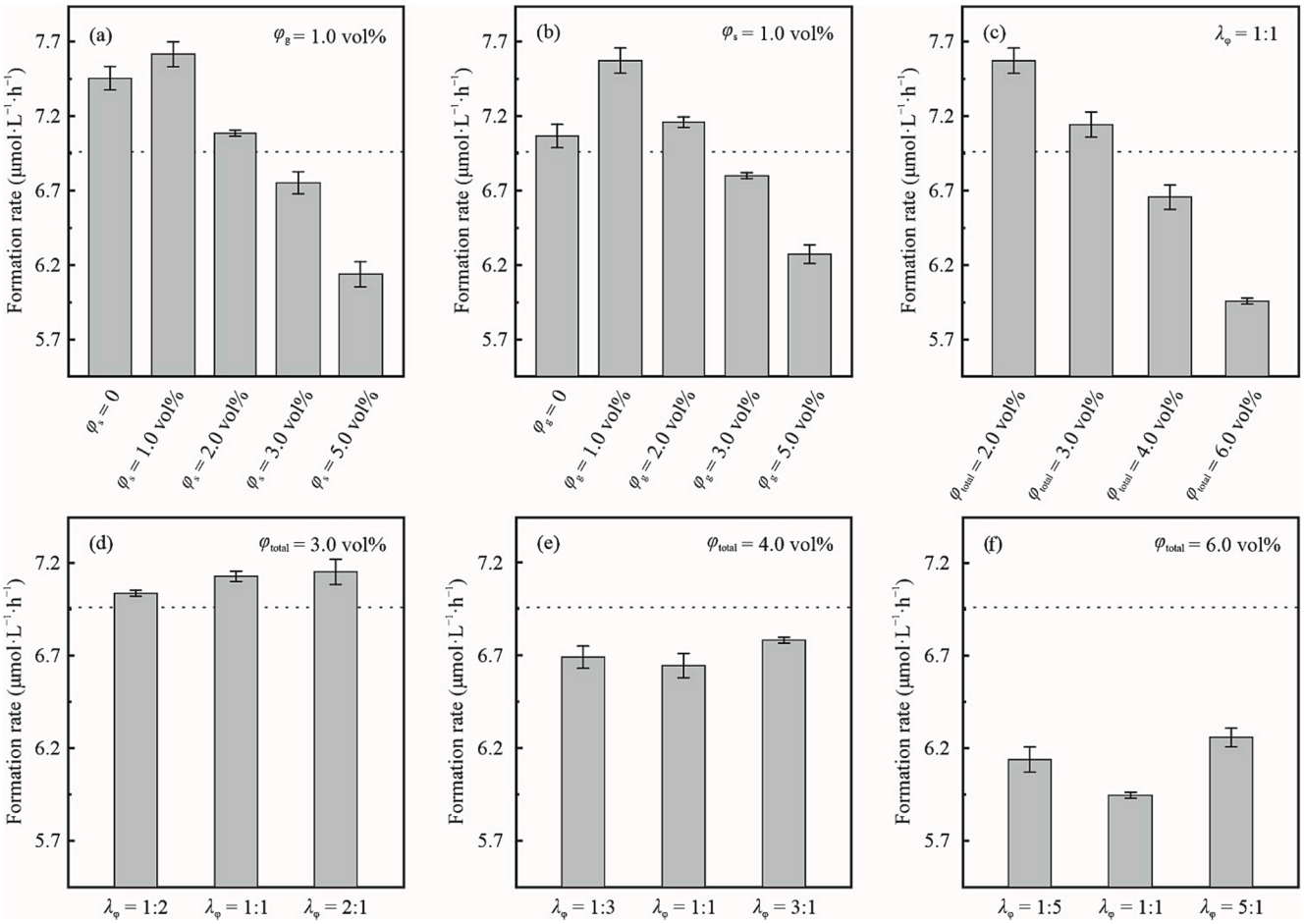

Fig. 7. Comparison of the I_3^- formation rates among the three-phase mixtures with (a) the same gas volume fraction (φ_g = 1.0 vol%) but different solids fractions (φ_s = 0–5.0 vol%); (b) the same φ_s (1.0 vol%) but different φ_g (0–5.0 vol%); (c) equal proportions of argon and silica (λ_φ = 1:1) but different total volume fractions (φ_{total} = 2.0–6.0 vol%); and the same φ_{total} but different λ_φ: (d) φ_{total} = 3.0 vol%, λ_φ = 1:2 to 2:1, (e) φ_{total} = 4.0 vol%, λ_φ = 1:3 to 3:1, and (f) φ_{total} = 6.0 vol%, λ_φ = 1:5 to 5:1. The dashed line represents the absence of silica particles and argon gas bubbles.

respectively. When the volume ratio of the gas phase and the solid phase was equal (λ_φ = 1:1), values of $r_f(I_3^-)$ at φ_{total} = 2.0 and 3.0 vol% was larger than that in the case with only the liquid phase, whereas at high φ_{total}, I_3^- was produced at a low rate (Fig. 7c). The marked decline in $r_f(I_3^-)$ with increasing φ_{total} from 2.0 to 6.0 vol% demonstrates the combined effects of gas and solid phases in inhibiting sonoreactions at high φ_g and φ_s. A clear distinction existed between the values of $r_f(I_3^-)$ at φ_{total} = 3.0 vol% (Fig. 7d) and those at φ_{total} = 4.0 and 6.0 vol% (Fig. 7e and f) with various λ_φ. When φ_{total} = 3.0 vol%, the sonochemical effects were enhanced at all λ_φ considered, and a higher proportion of gas bubbles seems to have improved enhancing effects. Contrastingly, at φ_{total} = 4.0 and 6.0 vol%, I_3^- formation was inhibited in all cases, with the largest $r_f(I_3^-)$ values at $\lambda_\varphi > 1$ and smallest at λ_φ = 1:1 (Fig. 7f). The inhibition mechanism will be discussed in the following section.

4. Discussion

The inhibition in sonochemical activity caused by solid particles and gas bubbles can be attributed to several possible mechanisms: (a) the addition of solid particles increased the apparent viscosity of the mixture, which could in turn lead to increased bubble oscillation time [65] and the formation of larger bubbles due to coalescence [66], thereby retarding the cavitation rates. (b) When the non-condensable argon gas diffused into cavitation bubbles, it could strongly influence the bubble dynamics, e.g., by decelerating the bubble collapse, weakening the shockwaves emitted, and reducing the intensity of cavitation [67]. This cushioning effect also accounts for the alleviation of cavitation damage to dam spillways by installing aerators [53,54]. (c) The presence of large amounts of solid particles and gas bubbles in the immediate vicinity of the ultrasonic horn (especially near the horn tip surface) could produce decoupling losses, minimizing the transfer of energy into the solution and decreasing the energy for the cavitation events [50]. (d) When ultrasound propagated in gas–solid–liquid mixtures, the gas and solid phases could also result in increased energy dissipation, attenuating the ultrasound and leaving even less energy available for acoustic cavitation [45,52].

Among the possible mechanisms, the first one was neglected in this study as our φ_s values were far lower than 40–50 vol%, a range in which Stoian et al. [27] reported greatly enhanced slurry viscosity and decreased sonochemical yields with increasing φ_s. As regards the second and third ones, the cushioning and decoupling effects were somewhat limited, because the mass of argon gas that diffused into cavitation bubbles was not directly related to the quantity of rising gas bubbles, and the localized decoupling loss made up only a small proportion of the total energy loss.

To understand the fourth mechanism, the acoustics of gas–solid–liquid mixtures should be examined at different concentrations of the gas and solid phases, from an energy perspective. The removal of acoustic energy in heterogeneous media is generally accepted to be caused by viscosity, scattering, and heat conductivity. Among the three main reasons, ultrasound attenuation in solid particle suspensions is primarily induced by scattering [55,56], whereas thermal

conduction plays the most important role in bubbly liquids [68,69]. Given the different regimes, we consider the total attenuation coefficient of the gas–solid–liquid mixtures, α_{total}, as the combination of the attenuation due to the solid particles, α_s, and that due to the gas bubbles, α_g, i.e.,

$$\alpha_{\text{total}} = \alpha_s + \alpha_g \tag{3}$$

Based on the one-dimensional two-phase hydrodynamic equations and linear perturbation analysis, Atkinson and Kytömaa [57] modeled sound propagation in monodisperse sphere suspensions and obtained a seemingly complex formula for α_s. With further algebraic simplification, we can reduce their formula to:

$$\alpha_s \approx \pi f \sqrt{\frac{\overline{\rho}}{\overline{\kappa}}}\left(1 - \frac{\rho_s \rho_l}{\overline{\rho}\rho^*}\right)\frac{A}{A^2 + (1-B)^2} \tag{4}$$

$$A = \frac{9\rho_l}{4\varphi_l \rho^*}\left(1 + \frac{\delta_s}{R_s}\right)\frac{\delta_s}{R_s} \tag{5}$$

$$B = \frac{9\rho_l}{4\varphi_l \rho^*}\left(\frac{4}{9}\zeta + \frac{\delta_s}{R_s}\right) \tag{6}$$

in which f is the ultrasound frequency; ρ_s and ρ_l are the densities of the solid particles and the liquid, respectively; $\delta_s = [\mu_l/(\pi f \rho_l)]^{1/2}$ is the viscous boundary layer thickness of the solid particles, where μ_l is the liquid viscosity; R_s is the radius of solid particles; $\zeta = \varphi_l/2$ is a simplified added mass coefficient; and the quantities $\overline{k}$, $\overline{\rho}$, and ρ^* are given by $\overline{k^{-1}} = \varphi_s \kappa_s^{-1} + \varphi_l \kappa_l^{-1}$, $\overline{\rho} = \varphi_s \rho_s + \varphi_l \rho_l$, and $\rho^* = \varphi_l \rho_s + \varphi_s \rho_l$, respectively, with κ_s and κ_l being the bulk moduli of the solid particles and the liquid, respectively. The model requires no viscous interactions between particles, which is satisfied in the limit that $\delta \ll h/2$, where $h = [(\varphi_s/\varphi_m)^{-1/3} - 1]R_s$ is the average interparticle spacing, and $\varphi_m \approx 64$ vol% is the maximum packing fraction for monodisperse spheres [70]. As $\delta_s \approx 0.1$ μm and $h/2$ ranges from 33 μm to 101 μm in the current study, the viscous boundary layers that surround the adjacent particles cannot overlap, and the model can be used.

In contrast to the limited variation of the sound speed in the solid particle suspensions, the speed of sound can be considerably lower in bubbly liquids than in either gas or liquid alone [71]. Brennen [72] simplified the phase velocity of ultrasound in the bubbly liquid, c, as

$$\frac{1}{c^2} = \frac{\varphi_g}{\gamma_g p_a}\left(\varphi_g \rho_g + \varphi_l \rho_l\right) \tag{7}$$

in which γ_g is the heat capacity ratio for gas; p_a is the ambient pressure; and ρ_g is the density of the gas in the bubble. Based on Eq. (7), we can rewrite Silberman's formula for α_g [58] as

$$\alpha_g = \pi f \sqrt{\frac{\varphi_g \rho_m}{\gamma_g p_a}}\frac{\delta_*}{\delta_*^2 + \left(1 - f_*^2\right)^2} \tag{8}$$

in which $\rho_m = \varphi_g \rho_g + \varphi_l \rho_l$ is the mean density of the bubbly liquid; $f_* = f/f_R$, where f_R is the bubble resonant frequency given by the Minnaert formula $f_R = (3\gamma_g p_a/\rho_m)^{1/2}/(2\pi R_g)$ [73], with R_g being the bubble radius; and $\delta_* = \delta f_*^2$, where δ is the total damping constant of gas bubbles, which is the sum of the scattering term δ_r, the viscous damping term δ_v, and the thermal damping term δ_t. We assume that $\delta \approx \delta_t$ in Eq. (8) because the influence of thermal conduction is dominant. Eller [74] developed the following expression for δ_t based on the work by Devin [75]:

$$\delta_t = \frac{3\left(\gamma_g - 1\right)[X(\sinh X + \sin X) - 2(\cosh X - \cos X)]}{X^2(\cosh X - \cos X) + 3\left(\gamma_g - 1\right)X(\sinh X - \sin X)} f_*^{-2} \tag{9}$$

$$X = 2R_g\sqrt{\frac{\pi f \rho_g c_{pg}}{K_g}} \tag{10}$$

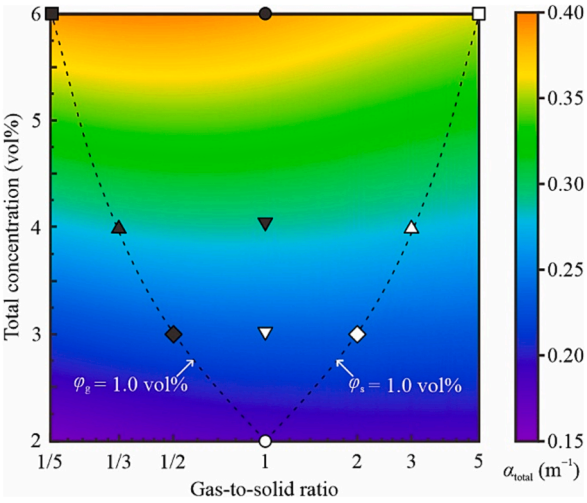

Fig. 8. Total acoustic attenuation coefficient (α_{total}) as a function of the total volume fraction and gas-to-solid ratio in three-phase mixtures, calculated using the following values (at 25 °C): (1) for/in water: $\rho_l = 1.0 \times 10^3$ kg·m^{-3}, $\mu_l = 0.89$ mPa·s, $\kappa_l = 2.2$ GPa, and $c = 1.5 \times 10^3$ m·s^{-1}; (2) for argon gas (bubbles): $R_g \approx 0.6$ mm, $\rho_g \approx 1.6$ kg·m^{-3}, $\gamma_g = 5/3$, $c_{pg} = 520.3$ J·kg^{-1}·K^{-1}, $K_g = 0.016$ W·m^{-1}·K^{-1}, and $p_a \approx 1.0 \times 10^5$ Pa; and (3) for silica particles: $R_s = 50$ μm, $\rho_s = 2.4 \times 10^3$ kg·m^{-3}, and $\kappa_s = 42.5$ GPa. The V-shaped dashed line represents acoustic attenuation at $\varphi_g = 1.0$ vol% (left) and $\varphi_s = 1.0$ vol% (right), and the markers correspond to the experimental cases in Table 1.

in which c_{pg} and K_g are the specific heat capacity (at constant pressure) and thermal conductivity of gas, respectively. As Domenico [59] opined, the model applies only to gas bubbles of $R_g > 0.15$ mm and far less than the sound wavelength. The gas bubble size in this study satisfies the requirements.

The calculations of the total attenuation using Eq. (3) are based on the assumption that the mutual interaction between the gas bubbles and the solid particles is insignificant, and the bubbles and particles advect with the ambient liquid velocity (no slip). This implies that, when calculating α_{total}, the volume fractions of separate phases in the expressions mentioned above should be revised by neglecting the presence of a third phase, i.e., replacing φ_s and φ_l in expressions for α_s by $\varphi_s/(1 - \varphi_g)$ and $(1 - \varphi_{\text{total}})/(1 - \varphi_g)$, and φ_g and φ_l in expressions for α_g by $\varphi_g/(1 - \varphi_s)$ and $(1 - \varphi_{\text{total}})/(1 - \varphi_s)$, respectively. Such revisions do not contradict the effective-medium approach when we neglect the bubble–particle interaction. It is reasonable to hypothesize, based on Fig. 3, that both the gas bubbles and the silica particles were uniformly sized and distributed in the solution in the calculation of α_{total}.

Eqs. (3)–(10) show that α_{total} is dependent on φ_g and φ_s. Fig. 8

Table 2
Calculated attenuation coefficients (gas–solid–liquid mixtures).

Case No.	φ_g[a] (vol%)	φ_s[b] (vol%)	α_g[c]	α_s[d]	α_{total}[e]
1	1.0	1.0	0.127	0.051	0.178
2	1.5	1.5	0.158	0.077	0.234
3	2.0	2.0	0.184	0.103	0.287
4	3.0	3.0	0.231	0.157	0.388
5	1.0	2.0	0.128	0.102	0.230
6	2.0	1.0	0.183	0.051	0.234
7	1.0	3.0	0.129	0.154	0.283
8	3.0	1.0	0.228	0.052	0.280
9	1.0	5.0	0.130	0.261	0.391
10	5.0	1.0	0.305	0.053	0.358

[a] φ_g—volume fraction of the argon gas bubbles.
[b] φ_s—volume fraction of the silica particles.
[c] α_g—acoustic attenuation coefficient due to the argon gas bubbles.
[d] α_s—acoustic attenuation coefficient due to the silica particles.
[e] α_{total}—total acoustic attenuation coefficient (sum of α_g and α_s).

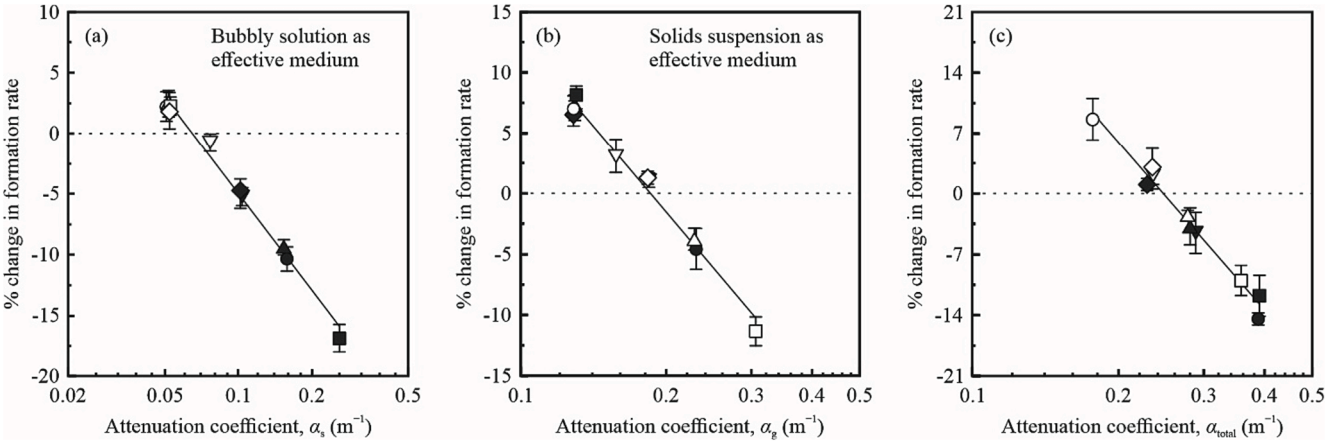

Fig. 9. Percentage change in I_3^- formation rate relative to (a) the bubbly solution, (b) the solids suspension, and (c) the pure water scenario, plotted against the attenuation coefficient due to the solid particles, α_s, the one due to the gas bubbles, α_g, and the total attenuation, α_{total}, respectively. The dashed lines represent no change in the formation rate of I_3^-, and the markers symbolize data for the experimental cases with the same shapes as in Fig. 8.

illustrates the relationships between acoustic attenuation and additive volume fractions in a filled contour map. At a fixed λ_φ, the increase in φ_{total} results in larger values of α_{total}, and consequently, a decline in $r_f(I_3^-)$ (Fig. 7c). α_{total} increases with φ_s when the bubbly water is deemed as an effective medium with φ_g being constant. Similarly, α_{total} increases with φ_g when φ_s is unchanged. However, the amount of increase in α_{total} with the same increments of additive addition is different in the two circumstances. For example, the increase in α_{total} caused by an increase in φ_s from 1.0 vol% to 5.0 vol% at $\varphi_g = 1.0$ vol% is 9% bigger than that caused by the same amount of increase in φ_g at $\varphi_s = 1.0$ vol%. This may explain why the decrease in $r_f(I_3^-)$ was sharper in Fig. 7(a) than in Fig. 7 (b). When φ_{total} is kept constant (>3.0 vol%), the variation of α_{total} with λ_φ is non-monotonic. As λ_φ increases, α_{total} first increases and then decreases, and such a trend is more pronounced at high φ_{total}. Among Cases 4, 9, and 10 in which $\varphi_{total} = 6.0$ vol%, the lowest value of α_{total} appears at $\lambda_\varphi = 5{:}1$, which can explain the highest I_3^- formation rate in Fig. 7(f).

Table 2 lists the calculation results of α_g, α_s, and α_{total} for all three-phase cases in Table 1. To nondimensionalize the measured formation rates of I_3^- in these cases, we define a percentage change in $r_f(I_3^-)$, β, as follows:

$$\beta = \frac{r_f(I_3^-) - r_{fo}(I_3^-)}{r_{fo}(I_3^-)} \times 100\% \tag{11}$$

in which $r_{fo}(I_3^-)$ is the formation rate of I_3^- in a selected case for reference. The case for reference can be the single-phase case in which silica particles and argon gas bubbles (both treated as additives in the three-phase case) were absent. It can also be a two-phase case if the effective-medium approach is adopted, regarding the third phase as the additive. The parameter β can be either positive (sonochemically enhancing) or negative (sonochemically inhibiting), with a value of zero representing no difference in sonochemical effects in comparison with the case for reference.

The strong negative relationships between β and the attenuation coefficients verify that ultrasound attenuation accounts for the inhibitory effects of gas bubbles and silica particles on sonoreactions, individually (Fig. 9a and b) and collectively (Fig. 9c). Although the gas and solid phases exhibited differences in the mechanisms of nucleus addition and acoustic attenuation, their sonochemically inhibiting effects were somewhat similar and combinative in three-phase mixtures at a relatively high φ_{total}. The sonochemical enhancement induced by introducing nuclei could be completely offset by inhibition when φ_{total} exceeded a critical value, which fell within 3.0–4.0 vol% under our test conditions (Fig. 7). Additional tests are required to analyze the critical φ_{total} in the future.

5. Conclusions

Sonochemical activity in aqueous solutions containing millimeter-sized argon gas bubbles and submillimeter-sized silica particles was experimentally investigated using an ultrasonic horn reactor (20 kHz). The effects of the volume fractions of the gas and solid phases were carefully examined, and the mechanism that underlies the sonochemically inhibiting effects of the two phases was clarified. The key findings and conclusions are as follows:

(a) The sonochemical yields decreased as the φ_{total} increased when the gas and solid phases had equal volume fractions. The sonoreactions were enhanced for all three cases at $\varphi_{total} = 3.0$ vol%, compared with the pure water case, and the yields increased with λ_φ. Contrastingly, the argon gas bubbles and silica particles had an inhibitory effect as the φ_{total} reached 4.0–6.0 vol%, with the highest and the lowest rates of radical production at $\lambda_\varphi > 1$ and $\lambda_\varphi = 1{:}1$, respectively.

(b) The model of the total acoustic attenuation is proposed (Eq. (3)), assuming that the bubble–particle interaction is insignificant. Two classic models, one considering scattering in solid particle suspensions (Eqs. (4)–(6)) and the other heat transfer in bubbly liquids (Eqs. (7)–(10)), are integrated into this model. The calculated α_{total} increases with φ_{total} for all λ_φ considered; when φ_{total} is kept constant (>3.0 vol%), α_{total} first increases and then decreases with increasing λ_φ.

(c) The percentage change in radical production, β, is a direct indicator of enhancing or inhibiting sonochemistry compared with the case for reference. Based on the effective-medium approach, we found that ·OH yields decreased with increasing φ_s, if φ_g was fixed, and vice versa. The experimentally determined β values correlate well with α_{total} that was theoretically calculated using our model, irrespective of whether the gas and solid phases were individually or collectively viewed.

Analyzing the sonochemical test results and ultrasound attenuation mechanisms in the gas–solid–liquid mixtures demonstrated that gas bubbles and solid particles in large quantities hold joint responsibility for inhibiting sonoreactions. An improved understanding of sonochemistry in three-phase mixtures would facilitate the scale-up of sonochemical reactors for practical wastewater treatment. The focus of future research should be on the size effects of the gas and solid phases.

CRediT authorship contribution statement

Kunpeng Su: Conceptualization, Formal analysis, Funding acquisition, Investigation, Methodology, Writing – original draft, Writing – review & editing. **Binghui Li:** Visualization, Data curation. **Jianhua Wu:** Supervision. **Pei Xin:** Supervision. **Shangtuo Qian:** Funding acquisition.

Declaration of Competing Interest

The authors declare that they have no known competing financial interests or personal relationships that could have appeared to influence the work reported in this paper.

Acknowledgements

This study was supported by the Natural Science Foundation of Jiangsu Province, China (Grant No. BK20230959), the National Natural Science Foundation of China (Grant No. 52279063), the Fundamental Research Funds for the Central Universities, China (Grant No. B220201043), and the Jiangsu Funding Program for Excellent Postdoctoral Talent (Grant No. 2022ZB163).

References

[1] M.H. Dehghani, R.R. Karri, J.R. Koduru, S. Manickam, I. Tyagi, N.M. Mubarak, Suhas, Recent trends in the applications of sonochemical reactors as an advanced oxidation process for the remediation of microbial hazards associated with water and wastewater: a critical review, Ultrason. Sonochem. 94 (2023), 106302, https://doi.org/10.1016/j.ultsonch.2023.106302.

[2] E.A. Serna-Galvis, J. Porras, R.A. Torres-Palma, A critical review on the sonochemical degradation of organic pollutants in urine, seawater, and mineral water, Ultrason. Sonochem. 82 (2022), 105861, https://doi.org/10.1016/j.ultsonch.2021.105861.

[3] F.V. de Andrade, R. Augusti, G.M. de Lima, Ultrasound for the remediation of contaminated waters with persistent organic pollutants: a short review, Ultrason. Sonochem. 78 (2021), 105719, https://doi.org/10.1016/j.ultsonch.2021.105719.

[4] K.S. Suslick, S.J. Doktycz, E.B. Flint, On the origin of sonoluminescence and sonochemistry, Ultrasonics 28 (5) (1990) 280–290, https://doi.org/10.1016/0041-624X(90)90033-K.

[5] R.J. Wood, J. Lee, M.J. Bussemaker, A parametric review of sonochemistry: Control and augmentation of sonochemical activity in aqueous solutions, Ultrason. Sonochem. 38 (2017) 351–370, https://doi.org/10.1016/j.ultsonch.2017.03.030.

[6] P.R. Gogate, A.B. Pandit, Sonochemical reactors: scale up aspects, Ultrason. Sonochem. 11 (3–4) (2004) 105–117, https://doi.org/10.1016/j.ultsonch.2004.01.005.

[7] T.J. Mason, Industrial sonochemistry: potential and practicality, Ultrasonics 30 (3) (1992) 192–196, https://doi.org/10.1016/0041-624X(92)90072-T.

[8] R.Y. Krishnan, S. Manikandan, R. Subbaiya, N. Karmegam, W. Kim, M. Govarthanan, Recent approaches and advanced wastewater treatment technologies for mitigating emerging microplastics contamination – a critical review, Sci. Total Environ. 858 (1) (2023), 159681, https://doi.org/10.1016/j.scitotenv.2022.159681.

[9] R. Herrmann-Heber, S.F. Reinecke, U. Hampel, Dynamic aeration for improved oxygen mass transfer in the wastewater treatment process, Chem. Eng. J. 386 (2020), 122068, https://doi.org/10.1016/j.cej.2019.122068.

[10] N.A. Oz, A.C. Uzun, Ultrasound pretreatment for enhanced biogas production from olive mill wastewater, Ultrason. Sonochem. 22 (2015) 565–572, https://doi.org/10.1016/j.ultsonch.2014.04.018.

[11] P.C. Sangave, A.B. Pandit, Ultrasound pre-treatment for enhanced biodegradability of the distillery wastewater, Ultrason. Sonochem. 11 (3–4) (2004) 197–203, https://doi.org/10.1016/j.ultsonch.2004.01.026.

[12] H.A. Meena, A. Garg, M. Kesharwani, Design of sewage treatment plant by act method, Int. J. Res. Appl. Sci. Eng. Tech. 7 (V) (2019) 1399–1403, https://doi.org/10.22214/ijraset.2019.5236.

[13] Y. Gu, Y. Li, F. Yuan, Q. Yang, Optimization and control strategies of aeration in WWTPs: a review, J. Clean. Prod. 418 (2023), 138008, https://doi.org/10.1016/j.jclepro.2023.138008.

[14] J. Choi, Y. Son, Quantification of sonochemical and sonophysical effects in a 20 kHz probe-type sonoreactor: Enhancing sonophysical effects in heterogeneous systems with milli-sized particles, Ultrason. Sonochem. 82 (2022), 105888, https://doi.org/10.1016/j.ultsonch.2021.105888.

[15] Y. Son, D. Lee, W. Lee, J. Park, W.H. Lee, M. Ashokkumar, Cavitational activity in heterogeneous systems containing fine particles, Ultrason. Sonochem. 58 (2019), 104599, https://doi.org/10.1016/j.ultsonch.2019.05.016.

[16] A. Nakajima, H. Sasaki, Y. Kameshima, K. Okada, H. Harada, Effect of TiO_2 powder addition on sonochemical destruction of 1,4-dioxane in aqueous systems, Ultrason. Sonochem. 14 (2) (2007) 197–200, https://doi.org/10.1016/j.ultsonch.2006.06.001.

[17] T. Tuziuti, K. Yasui, M. Sivakumar, Y. Iida, N. Miyoshi, Correlation between acoustic cavitation noise and yield enhancement of sonochemical reaction by particle addition, J. Phys. Chem. A 109 (21) (2005) 4869–4872, https://doi.org/10.1021/jp0503516.

[18] T. Tuziuti, K. Yasui, Y. Iida, H. Taoda, S. Koda, Effect of particle addition on sonochemical reaction, Ultrasonics 42 (1–9) (2004) 597–601, https://doi.org/10.1016/j.ultras.2004.01.082.

[19] A. Keck, E. Gilbert, R. Köster, Influence of particles on sonochemical reactions in aqueous solutions, Ultrasonics 40 (1–8) (2002) 661–665, https://doi.org/10.1016/S0041-624X(02)00195-6.

[20] G. Zhang, I. Hua, The impact of particulates on the aqueous sonication of bromobenzene, Chemosphere 46 (1) (2002) 59–66, https://doi.org/10.1016/S0045-6535(01)00079-0.

[21] Y. Lu, L.K. Weavers, Sonochemical desorption and destruction of 4-chlorobiphenyl from synthetic sediments, Environ. Sci. Technol. 36 (2) (2002) 232–237, https://doi.org/10.1021/es010641+.

[22] Y. Lu, N. Riyanto, L.K. Weavers, Sonolysis of synthetic sediment particles: particle characteristics affecting particle dissolution and size reduction, Ultrason. Sonochem. 9 (4) (2002) 181–188, https://doi.org/10.1016/S1350-4177(02)00076-7.

[23] S. Lee, Y. Son, Effects of gas saturation and sparging on sonochemical oxidation activity under different liquid level and volume conditions in 300-kHz sonoreactors: zeroth- and first-order reaction comparison using KI dosimetry and BPA degradation, Ultrason. Sonochem. 98 (2023), 106521, https://doi.org/10.1016/j.ultsonch.2023.106521.

[24] Y. Son, J. Seo, Effects of gas saturation and sparging on sonochemical oxidation activity in open and closed systems, Part I: H_2O_2 generation, Ultrason. Sonochem. 90 (2022), 106214, https://doi.org/10.1016/j.ultsonch.2022.106214.

[25] J. Choi, J. Khim, B. Neppolian, Y. Son, Enhancement of sonochemical oxidation reactions using air sparging in a 36 kHz sonoreactor, Ultrason. Sonochem. 51 (2019) 412–418, https://doi.org/10.1016/j.ultsonch.2018.07.032.

[26] T. Tuziuti, Influence of sonication conditions on the efficiency of ultrasonic cleaning with flowing micrometer-sized air bubbles, Ultrason. Sonochem. 29 (2016) 604–611, https://doi.org/10.1016/j.ultsonch.2015.09.011.

[27] D. Stoian, N. Eshtiaghi, J. Wu, R. Parthasarathy, Intensification of sonochemical reactions in solid–liquid systems under fully suspended condition, Chem. Eng. Process. 123 (2018) 34–44, https://doi.org/10.1016/j.cep.2017.10.025.

[28] A.A. Atchley, A. Prosperetti, The crevice model of bubble nucleation, J. Acoust. Soc. Am. 86 (3) (1989) 1065–1084, https://doi.org/10.1121/1.398098.

[29] K. Su, D. Xia, J. Wu, P. Xin, Y. Wang, Particle size distribution effects on cavitation erosion in sediment suspensions, Wear 518–519 (2023), 204629, https://doi.org/10.1016/j.wear.2023.204629.

[30] K. Su, J. Wu, D. Xia, Dual role of microparticles in synergistic cavitation–particle erosion: modeling and experiments, Wear 470–471 (2021), 203633, https://doi.org/10.1016/j.wear.2021.203633.

[31] D. Xia, K. Su, J. Wu, Z. Ding, Influence of solids motion on ultrasonic horn tip erosion in solid–liquid two-phase flows, Wear 480–481 (2021), 203928, https://doi.org/10.1016/j.wear.2021.203928.

[32] K. Su, J. Wu, D. Xia, Classification of regimes determining ultrasonic cavitation erosion in solid particle suspensions, Ultrason. Sonochem. 68 (2020), 105214, https://doi.org/10.1016/j.ultsonch.2020.105214.

[33] Y.T. Didenko, W.B. McNamara III, K.S. Suslick, Effect of noble gases on sonoluminescence temperatures during multibubble cavitation, Phys. Rev. Lett. 84 (4) (2000) 777–780, https://doi.org/10.1103/PhysRevLett.84.777.

[34] C. Petrier, A. Jeunet, J.L. Luche, G. Reverdy, Unexpected frequency effects on the rate of oxidative processes induced by ultrasound, J. Am. Chem. Soc. 114 (8) (1992) 3148–3150, https://doi.org/10.1021/ja00034a077.

[35] S. Kumari, M. Keswani, S. Singh, M. Beck, E. Liebscher, P. Deymier, S. Raghavan, Control of sonoluminescence signal in deionized water using carbon dioxide, Microelectron. Eng. 88 (12) (2011) 3437–3441, https://doi.org/10.1016/j.mee.2010.10.036.

[36] M.V. Bagal, P.R. Gogate, Sonochemical degradation of alachlor in the presence of process intensifying additives, Sep. Purif. Technol. 90 (2012) 92–100, https://doi.org/10.1016/j.seppur.2012.02.019.

[37] E.L. Mead, R.G. Sutherland, R.E. Verrall, The effects of ultrasound on water in the presence of dissolved gases, Can. J. Chem. 54 (7) (1976) 1114–1120, https://doi.org/10.1139/v76-159.

[38] S. Merouani, H. Ferkous, O. Hamdaoui, Y. Rezgui, M. Guemini, New interpretation of the effects of argon-saturating gas toward sonochemical reactions, Ultrason. Sonochem. 23 (2015) 37–45, https://doi.org/10.1016/j.ultsonch.2014.09.009.

[39] R. Pflieger, T. Chave, G. Vite, L. Jouve, S.I. Nikitenko, Effect of operational conditions on sonoluminescence and kinetics of H_2O_2 formation during the sonolysis of water in the presence of Ar/O_2 gas mixture, Ultrason. Sonochem. 26 (2015) 169–175, https://doi.org/10.1016/j.ultsonch.2015.02.005.

[40] Y. Ono, K. Shinashi, H. Tanaka, H. Harada, Mechanism of improving the rate of sono-oxidation of a KI solution by introduction of CO_2 into an Ar atmosphere, Ultrason. Sonochem. 51 (2019) 145–150, https://doi.org/10.1016/j.ultsonch.2018.10.033.

[41] S.N. Katekhaye, P.R. Gogate, Intensification of cavitational activity in sonochemical reactors using different additives: efficacy assessment using a model reaction, Chem. Eng. Process. 50 (2011) 95–103, https://doi.org/10.1016/j.cep.2010.12.002.

[42] N. Shimizu, C. Ogino, M.F. Dadjour, K. Ninomiya, A. Fujihira, K. Sakiyama, Sonocatalytic facilitation of hydroxyl radical generation in the presence of TiO_2,

Ultrason. Sonochem. 15 (6) (2008) 988–994, https://doi.org/10.1016/j.ultsonch.2008.04.011.
[43] N. Her, J.-S. Park, Y. Yoon, Sonochemical enhancement of hydrogen peroxide production by inert glass beads and TiO_2-coated glass beads in water, Chem. Eng. J. 166 (1) (2011) 184–190, https://doi.org/10.1016/j.cej.2010.10.059.
[44] A. Barchouchi, S. Molina-Boisseau, N. Gondrexon, S. Baup, Sonochemical activity in ultrasonic reactors under heterogeneous conditions, Ultrason. Sonochem. 72 (2021), 105407, https://doi.org/10.1016/j.ultsonch.2020.105407.
[45] K. Su, J. Wu, D. Xia, X. Zhang, Clarification of regimes determining sonochemical reactions in solid particle suspensions, Ultrason. Sonochem. 82 (2022), 105910, https://doi.org/10.1016/j.ultsonch.2022.105910.
[46] H. Ge, J. Li, H.S. Chen, Influence of microparticle size on cavitation noise during ultrasonic vibration, AIP Adv. 5 (2015), 097145, https://doi.org/10.1063/1.4931162.
[47] T. Tuziuti, K. Yasui, T. Kozuka, A. Towata, Y. Iida, Enhancement of sonochemical reaction rate by addition of micrometer-sized air bubbles, J. Phys. Chem. A 110 (37) (2006) 10720–10724, https://doi.org/10.1021/jp063373g.
[48] T. Tuziuti, K. Yasui, M. Sivakumar, Y. Iida, Influence of dissolved-air concentration on spatial distribution of bubbles for sonochemistry, Ultrasonics 44 (2006) 357–361, https://doi.org/10.1016/j.ultras.2006.05.002.
[49] J. Choi, H. Lee, Y. Son, Effects of gas sparging and mechanical mixing on sonochemical oxidation activity, Ultrason. Sonochem. 70 (2021), 105334, https://doi.org/10.1016/j.ultsonch.2020.105334.
[50] P.R. Gogate, S. Shaha, L. Csoka, Intensification of cavitational activity in the sonochemical reactors using gaseous additives, Chem. Eng. J. 239 (2014) 364–372, https://doi.org/10.1016/j.cej.2013.11.004.
[51] P.R. Gogate, S. Shaha, L. Csoka, Intensification of cavitational activity using gases in different types of sonochemical reactors, Chem. Eng. J. 262 (2015) 1033–1042, https://doi.org/10.1016/j.cej.2014.10.074.
[52] D. Xia, J. Wu, K. Su, Influence of micron-sized air bubbles on sonochemical reactions in aqueous solutions exposed to combined ultrasonic irradiation and aeration processes, J. Environ. Chem. Eng. 10 (6) (2022), 108685, https://doi.org/10.1016/j.jece.2022.108685.
[53] J. Wu, K. Su, Y. Wang, W. Gou, Effect of air bubble size on cavitation erosion reduction, Sci. China Technol. Sci. 60 (2017) 523–528, https://doi.org/10.1007/s11431-016-0593-5.
[54] S.O. Russell, G.J. Sheehan, Effect of entrained air on cavitation damage, Can. J. Civ. Eng. 1 (1) (1974) 97–107, https://doi.org/10.1139/l74-008.
[55] P.S. Epstein, R.R. Carhart, The absorption of sound in suspensions and emulsions. I. Water fog in air, J. Acoust. Soc. Am. 25 (3) (1953) 553–565, https://doi.org/10.1121/1.1907107.
[56] J.R. Allegra, S.A. Hawley, Attenuation of sound in suspensions and emulsions: theory and experiments, J. Acoust. Soc. Am. 51 (5B) (1972) 1545–1564, https://doi.org/10.1121/1.1912999.
[57] C.M. Atkinson, H.K. Kytömaa, Acoustic wave speed and attenuation in suspensions, Int. J. Multiphas. Flow 18 (4) (1992) 577–592, https://doi.org/10.1016/0301-9322(92)90053-J.
[58] E. Silberman, Sound velocity and attenuation in bubbly mixtures measured in standing wave tubes, J. Acoust. Soc. Am. 29 (8) (1957) 925–933, https://doi.org/10.1121/1.1909101.
[59] S.N. Domenico, Acoustic wave propagation in air-bubble curtains in water—Part I: history and theory, Geophysics 47 (3) (1982) 345–353, https://doi.org/10.1190/1.1441340.
[60] D.A. Gubaidullin, Y.V. Fedorov, Acoustics of a viscoelastic medium with encapsulated bubbles, J. Hydrodyn. 33 (2021) 55–62, https://doi.org/10.1007/s42241-021-0003-2.
[61] S.I. Nikitenko, C. Le Naour, P. Moisy, Comparative study of sonochemical reactors with different geometry using thermal and chemical probes, Ultrason. Sonochem. 14 (3) (2007) 330–336, https://doi.org/10.1016/j.ultsonch.2006.06.006.
[62] S. Merouani, O. Hamdaoui, F. Saoudi, M. Chiha, Influence of experimental parameters on sonochemistry dosimetries: KI oxidation, Fricke reaction and H_2O_2 production, J. Hazard. Mater. 178 (1–3) (2010) 1007–1014, https://doi.org/10.1016/j.jhazmat.2010.02.039.
[63] J. Choi, Y. Son, Effect of dissolved gases on sonochemical oxidation in a 20 kHz probe system: continuous monitoring of dissolved oxygen concentration and sonochemical oxidation activity, Ultrason. Sonochem. 97 (2023), 106452, https://doi.org/10.1016/j.ultsonch.2023.106452.
[64] Y. Son, Y. No, J. Kim, Geometric and operational optimization of 20-kHz probe-type sonoreactor for enhancing sonochemical activity, Ultrason. Sonochem. 65 (2020), 105065, https://doi.org/10.1016/j.ultsonch.2020.105065.
[65] Y.S. Kannan, S. Balusamy, B. Karri, K.C. Sahu, Effect of viscosity on the dynamics of a non-equilibrium bubble in free-field and near a free-surface, Exp. Therm. Fluid Sci. 116 (2020), 110113, https://doi.org/10.1016/j.expthermflusci.2020.110113.
[66] A. Tagawa, N. Dohi, Y. Kawase, Volumetric gas−liquid mass transfer coefficient in aerated stirred tank reactors with dense floating solid particles, Ind. Eng. Chem. Res. 51 (4) (2012) 1938–1948, https://doi.org/10.1021/ie1023222.
[67] T. Trummler, S.J. Schmidt, N.A. Adams, Numerical investigation of non-condensable gas effect on vapor bubble collapse, Phys. Fluids 33 (2021), 096107, https://doi.org/10.1063/5.0062399.
[68] D.A. Gubaidullin, Y.V. Fedorov, Acoustic waves in a liquid with solid particles and gas bubbles, Fluid Dyn. 53 (2018) 248–254, https://doi.org/10.1134/S0015462818020088.
[69] A. Prosperetti, Thermal effects and damping mechanisms in the forced radial oscillations of gas bubbles in liquids, J. Acoust. Soc. Am. 61 (1977) 17–27, https://doi.org/10.1121/1.381252.
[70] V. Baranau, U. Tallarek, Random-close packing limits for monodisperse and polydisperse hard spheres, Soft Matter 10 (2014) 3826–3841, https://doi.org/10.1039/C3SM52959B.
[71] P.S. Wilson, R.A. Roy, An audible demonstration of the speed of sound in bubbly liquids, Am. J. Phys. 76 (2008) 975–981, https://doi.org/10.1119/1.2907773.
[72] C.E. Brennen, Chapter 6 - Homogeneous bubbly flows, in: Cavitation and Bubble Dynamics, Cambridge University Press, 2013, pp. 145–181, https://doi.org/10.1017/CBO9781107338760.007.
[73] M. Minnaert, XVI. On musical air-bubbles and the sounds of running water, Lond. Edinb. Dublin Philos. Mag. 16(104) (1933) 235–248, https://doi.org/10.1080/14786443309462277.
[74] A.I. Eller, Damping constants of pulsating bubbles, J. Acoust. Soc. Am. 47 (1970) 1469–1470, https://doi.org/10.1121/1.1912063.
[75] C. Devin, Survey of thermal, radiation, and viscous damping of pulsating air bubbles in water, J. Acoust. Soc. Am. 31 (12) (1959) 1654–1667, https://doi.org/10.1121/1.1907675.